Surface-Enhanced Raman Scattering: Comparison of Three Different Molecules on Single-Crystal Nanocubes and Nanospheres of Silver†

Matthew Rycenga,‡ Moon Ho Kim,‡ Pedro H. C. Camargo,‡ Claire Cobley,‡ Zhi-Yuan Li,§ and Younan Xia*,‡

Department of Biomedical Engineering, Washington University, St. Louis, Missouri 63130, and Institute of Physics, Chinese Academy of Sciences, Beijing 100080, P. R. China

Received: November 19, 2008; Revised Manuscript Received: December 27, 2008

We have investigated the surface-enhanced Raman scattering (SERS) of chemically prepared single-crystal nanocubes and nanospheres of Ag with three different molecules to quantitatively understand the effect of sharp features on the SERS enhancement factor. Both experimental measurements and theoretical calculations confirmed a higher SERS activity for the nanocubes as a result of sharp features on their surfaces. We also found major discrepancies between the measured SERS intensities and those predicted from the electromagnetic mechanism. Through analysis of SERS bands, we concluded that sharp features on the Ag nanocubes could greatly increase the contribution of the chemical enhancement to the SERS intensity.

Introduction

Surface-enhanced Raman scattering (SERS) is a technique that greatly enhances the Raman scattering cross-sections for molecules in the vicinity of metallic nanostructures.[1] The metallic structures are essential for SERS, as their localized surface plasmon resonances can amplify Raman signals by many orders of magnitude.[2] SERS is truly a nanoscale phenomenon, and its dependence on a myriad of subtle parameters, often at the nanoscale, has made it a challenging subject to study, control, and model. Yet, SERS has been shown to have the remarkable capability to detect molecules at extraordinarily low concentrations, even single molecules, making this technique unique and extremely useful in numerous venues.[3−5] While initial investigations of SERS were concerned with observing and recording the SERS signals with an effort to simply maximize the SERS effect, the current emphasis rests on understanding the fundamental aspects of SERS. This is essential for the rational design of nanostructures that will give rise to a paramount SERS effect.[6] In most of these studies, however, what has remained constant is the empirical indicator of the prominence of a specific SERS system, namely the enhancement factor (EF). The EF explicitly denotes the magnitude of the enhancement in a SERS measurement. It is extremely important for applications of SERS devices and also for comparison with theory. Its importance is often mired by differences in the definition of the EF and how it is actually calculated. This fact has inspired critiques and studies of the EF for numerous situations.[7,8] In the present study, we focus on metallic nanoparticles of Ag with cubic and spherical shapes and compare these two substrates with respect to their calculated EFs.

The use of metallic nanoparticles in SERS has a long history which includes the first examples of single-molecule detection.[9,10] These systems have given rise to the notion of hot spots (regions where extraordinary SERS intensities are generated), and subsequent simulations have fueled a great number of fundamental and practical studies into the role nanoscale gaps and features play in SERS.[11−14] While experiments are beginning to come to terms with simulations of gaps and holes,[15] there has been no coherent experimental corroboration with theory that suggests sharp nanoscale features can provide stronger Raman scattering than smoother ones. Past studies have primarily viewed the geometrical morphology of a nanoparticle as a handle for controlling the frequency of the plasmon resonance. These studies have confirmed the notion that, in general, the most intense SERS is observed when the nanoparticle's surface plasmon is in resonance with the incident radiation.[16−18] However, the geometry of a metal nanoparticle not only imparts the defined plasmon resonant frequencies but also determines the spatial distribution and extent of the near-field polarization dependencies and even how molecules interact with the nanoparticle. Theoretical calculations predict that local electric fields around a nanoparticle will be confined to corners or sharp points, thereby increasing their SERS intensity.[11] Yet, the question of how significant this parameter is, particularly with respect to holes and gaps, remains undetermined and is anticipated to be relatively modest.[12] To this end, single-crystal nanocubes and nanospheres of Ag were prepared for SERS to provide a clear example of this dependency. Our study reveals some dependencies of SERS on sharp nanoscale features by providing insight into the factors that contribute to high SERS intensities, information that will undoubtedly be useful for the rational design of nanostructures for SERS applications.

Experimental Section

Chemicals and Materials. Silver nitrate ($AgNO_3$, 99%), poly(vinyl pyrrolidone) (PVP, $M_n \approx 55\,000$), 4-methylbenzenethiol (4-MBT, 98%), and 1-pentanethiol (1-PT, 98%) were all obtained from Sigma-Aldrich and used as received. Ethylene glycol (EG) and sodium sulfide (Na_2S, 99%) were obtained from J. T. Baker, and 1,4-benzenedithiol (1,4-BDT, 98%) was obtained from Alfa Aesar. Ethanol (200 proof) was obtained from Pharmco Products Inc. All aqueous solutions were prepared with deionized water (18.1 MΩ cm).

Particle Synthesis and Characterization. The Ag nanocubes and Ag nanospheres were synthesized using the polyol method

† Part of the George C. Schatz Festschrift.

* Corresponding author. E-mail: xia@biomed.wustl.edu.
‡ Washington University.
§ Chinese Academy of Sciences.

10.1021/jp8101817 CCC: $40.75
Published on Web 01/28/2009

where $AgNO_3$ is reduced in EG to elemental Ag and directed to grow into a specific shape. The polyol-based synthesis of Ag nanocubes has been developed into a robust method, and a detailed protocol can be found elsewhere.[19] In brief, the Ag nanocubes were synthesized by reduction of $AgNO_3$ with EG in the presence of PVP and Na_2S. Following synthesis, the Ag nanocubes were isolated by centrifugation, washed with water to remove EG and excess PVP, and, finally, dispersed in water for storage. The Ag nanospheres were also prepared using the polyol method, but in the presence of NaCl rather than Na_2S. A detailed protocol can be found elsewhere.[20]

The nanocubes and nanospheres were characterized by scanning electron microscopy (SEM), where the samples were prepared by drying aqueous suspensions of the nanoparticles on silicon substrates under ambient conditions. SEM images were taken using a field-emission microscope operated at 15 kV. A JEOL 2100F high-resolution tunneling electron microscope (HRTEM) operated at 200 kV was also used to take images of the nanoparticles. Nanocube and nanosphere dimensions were obtained from the SEM images using ImageJ (Wayne Rasband, NIH) software. The localized surface plasmon resonance (LSPR) of the nanoparticles were determined with a Varian Cary 50 UV−vis spectrophotometer equipped with a tungsten lamp. For each sample, the nanoparticle concentration was estimated by determining the Ag^+ concentration with ICP-MS (Agilent 7500ce inductively coupled plasma spectrometer) and using this knowledge with the nanoparticle dimensions from SEM imaging. The error associated with determining the silver ion concentration (the instrumental error and sample preparation) was near 5%.

The nanoparticles were functionalized with a 1 mM ethanol solution of the thiol over a period of 24 h. Ethanol was used to wash the sample several times before resuspending the sample in water to achieve a concentration of 0.5−3 nM of Ag nanocubes or nanospheres.

Normal Raman Spectroscopy. Normal Raman spectroscopy was recorded with solutions of ∼10 mM 1,4-BDT or 4-MBT in basic NaOH (∼6 M), where the molecule is in an anionic form and much more soluble in water. For 1-PT, the normal Raman spectrum was taken with the neat liquid. For these samples, $\lambda_{ex} = 514$ nm, $P_{laser} = 4.3$ mW, and $t = 30$ s.

Surface-Enhanced Raman Scattering. The Raman spectra were recorded from a solution phase using a Renishaw inVia confocal Raman spectrophotometer coupled to a Leica microscope with an 50× objective (NA = 0.90) in backscattering configuration. The 514 nm wavelength was generated from an argon laser and used with a holographic notch filter based on a grating of 1200 lines per millimeter. The backscattered Raman signals were collected on a thermoelectrically cooled (−60 °C) CCD detector. Sample cells were constructed by attaching the caps of microcentrifuge tubes to glass slides. The cap acted as a vessel for the liquid sample, and glass coverslips (0.17−0.13 mm) were carefully placed on top to eliminate solvent evaporation and to act as a reference point from which the focal volume was lowered to a depth of 200 μm into the sample. SERS data was collected with $\lambda_{ex} = 514$ nm, $P_{laser} = 4.1$ mW, and $t = 10$ s.

Processing of the Raman spectra and all data analysis was done with IGOR Pro software (Portland, OR). All data was baseline corrected before normalization. For the baseline correction a fourth-order polynomial was fitted to the raw Raman spectrum and subtracted. Vector normalization was done by calculating the sum of the squared intensity values of the spectrum and using the squared root of this sum as the normalization constant.[21] Peak areas, not intensities, were used for data analysis. Lorentzian fits for the Raman modes were found with IgorPro MultiPeakFit software. A cubic polynomial baseline defined by the fit program was used. Four variables were fit, including the area, peak amplitude, width, and the center of frequency. Goodness of fit was gauged by comparing the standard deviation (σ) of the fit parameters with $\sigma < 15\%$.

Determination of the Enhancement Factor. A significant problem in determining the EF is its dependence on the number of molecules in the scattering volume.[7] Without knowing this parameter, interpreting the measured EF can be difficult. To attenuate this problem, 1,4-BDT, 4-MBT, and 1-PT were used to determine the EF as these molecules bind to the metal surface in a known way and form only a monolayer.[22−25] This was confirmed through SERS by periodically checking for S−H stretching bands (∼2550 cm^{-1} for the benzenethiols and 2575 cm^{-1} for 1-PT) and S−S stretching bands (∼530 cm^{-1}), as these bands would develop in a multilayer. The Supporting Information (Tables S1−S3) lists the Raman bands that were observed in this study for each of these molecules. The EF was calculated using eq 1 shown below

$$\mathrm{EF} = \frac{I_{\mathrm{SERS}}}{I_{\mathrm{Bulk}}} \times \frac{N_{\mathrm{Bulk}}}{N_{\mathrm{ads}}} \tag{1}$$

where N_{Bulk} is the number of molecules in the scattering volume for the normal Raman measurement and N_{ads} is the number of adsorbed molecules in the scattering volume for SERS. I_{SERS} is the peak area of a band from the SERS measurement and I_{Bulk} is the peak area of the same band from the normal Raman measurement. A sample EF calculation is provided in the Supporting Information. We have quantified the error in eq 1 by extrapolating the errors associated with the standard deviation of the Lorentzian peak fit and uncertainties in the calculated concentrations. We found that the error associated with eq 1 is about 20% for all the calculated average EFs.

Theoretical Calculations. The discrete-dipole approximation (DDA) method[26] was used to calculate the far-field extinction spectra and the near-field distributions at an excitation wavelength of 514 nm for the Ag nanocubes. We used 64 000 dipoles to approximate the nanocube at different polarizations to account for the nanocube's random orientation to the laser polarization. For the Ag sphere, Mie theory was employed to calculate the extinction spectra as well as the near-field distribution when the sphere is irradiated at a wavelength of 514 nm. All calculations were performed for particles in an external dielectric medium of water.

Results and Discussion

The polyol method for synthesis of noble-metal nanocrystals has been developed to a point where many well-defined shapes are now available as uniform samples and in relatively large quantities.[27] This, coupled with the sophistication of current electromagnetic simulations of light-particle interactions, has enabled the synthesis of nanoparticles with predetermined spectral attributes.[28] Figure 1 shows SEM and TEM images of the particles used in this study that were synthesized using the polyol method. The objective of this work is to closely compare the SERS of nanocubes, with eight sharp corners, to nanospheres, which have no sharp features. Figure 2 shows the normalized experimental and calculated extinction spectra for Ag nanocubes and nanospheres. It is worth pointing out that only recently have we been able to generate single-crystal nanospheres as uniform samples by modifying the polyol method for truncated Ag nanocubes that involved the use of

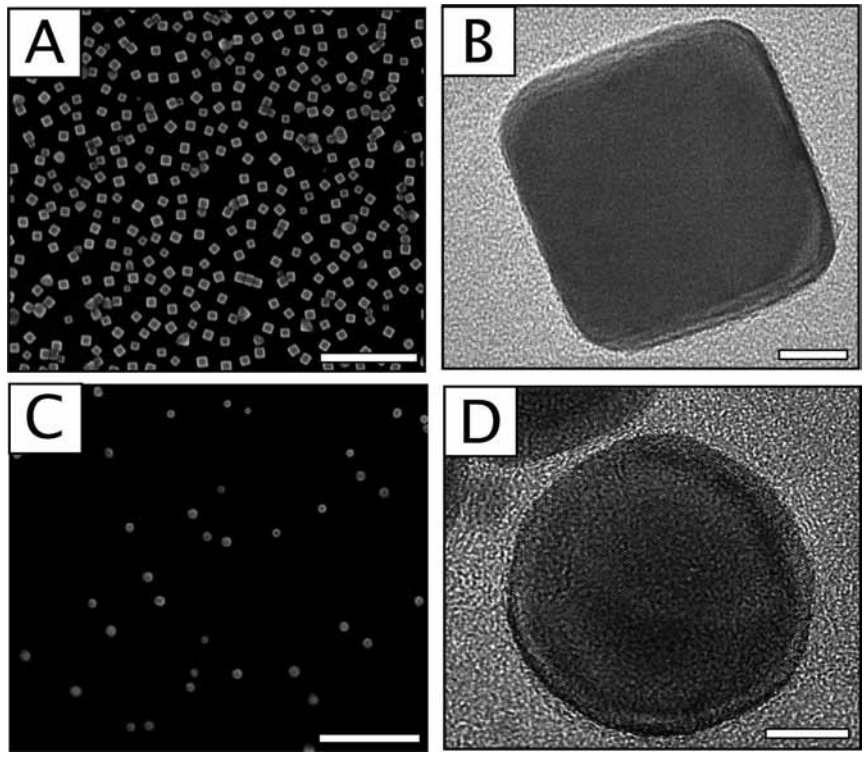

Figure 1. SEM images (A, C) and TEM images (B, D) of the Ag nanocubes and Ag nanospheres used for SERS measurements in this study. The nanocubes, shown in parts A and B, had an average edge length of 38 ± 8 nm. The nanospheres, shown in parts C and D, had an average diameter of 35 ± 7 nm. The scale bars correspond to 1 μm in A and C and 10 nm in B and D.

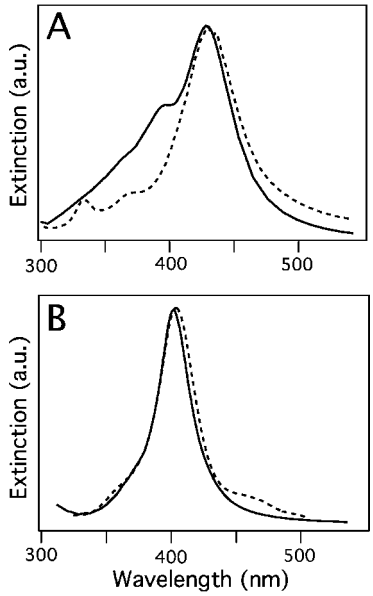

Figure 2. The calculated far-field extinction spectra (solid) and the experimentally measured extinction spectra (dashed) for Ag nanocubes 38 nm in edge length (A) and Ag nanospheres 35 nm in diameter (B). All spectra were calculated or measured for particles suspended in water. The main extinction peak was located at 440 nm for the nanocubes and 410 nm for the nanospheres.

oxygen and chloride.[20] Although these structures were actually truncated octahedrons, they had the most spherical shape possible for single-crystal Ag nanoparticles and had the same far-field properties as simulated for nanospheres of similar sizes (see Figure 2B). Note that the simulated extinction spectra were in good agreement with the experimentally determined spectra for the particles used in this study. In Figure 2A, the shoulder at 390 nm seems to originate from the splitting of the original dipole resonance peak for a small silver nanocube as a result of the sharp corners.[29]

We recorded the SERS of three different molecules chemisorbed onto nanocubes and nanospheres, as seen in Figure 3. The molecules used in this study, 1,4-BDT, 4-MBT, and 1-PT, readily adsorb to the silver suface through a thiolate bond, forming a monolayer which has been, in general, well characterized.[22,25,30] This allows us to predict how many molecules are adsorbed on each nanoparticle and the orientation of the molecule on the surface of the nanoparticle. This information, along with the nanoparticle concentration (see Supporting Information), allows us to estimate the number of molecules that we were sampling with each acquisition.

The SERS measurement that is of interest to this study is the average EF experienced by a molecule on either a nanocube or nanosphere. The EFs presented herein are averages for three reasons: (i) the nanoparticles have no specific orientation relative to the polarization of the excitation source, (ii) our SERS data originates from the entire surface of the nanoparticle (i.e., this study does not involve single molecules or isolation of "hot spots"), and (iii) the measurement involves many hundreds of nanoparticles. The average EFs calculated for the nanocubes and nanospheres are summarized in Table 1. A detailed calculation can be found in the Supporting Information. Table 1 also shows the expected orientation of the molecule on the Ag nanoparticle surface. 1,4-BDT has been shown to form a monolayer with both sulfur groups forming a thiolate bond on the Ag surface.[30] This puts the benzene ring of the molecule in close proximity to the surface of the nanoparticle. In contrast, 4-MBT forms only one thiolate bond and is believed to form a monolayer semiperpendicular to the metal surface.[22,31] Like other alkanethiols, 1-PT forms a well-defined self-assembled monolayer, with the sulfur group forming a thiolate bond and neighboring alkane chains forming cohesion bonds through van

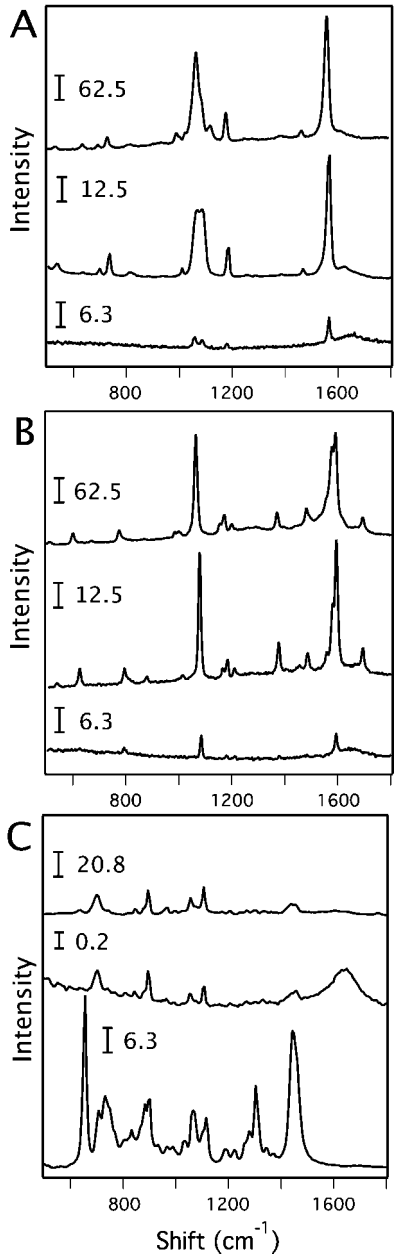

Figure 3. SERS spectra taken from nanocubes 38 nm in edge length (top trace) and nanospheres 35 nm in diameter (middle trace) and the normal Raman scattering spectra (bottom trace), for three different molecules: (A) 1,4-BDT, (B) 4-MBT, and (C) 1-PT. The numbers above each spectrum represent the scale in adu mW^{-1} s^{-1}. In part C, the peak at 1640 cm^{-1} is from water and is present because of the low Raman intensity of 1-PT on nanospheres.

der Walls interactions.[32] These molecules were used as probes to determine the average EFs of both the nanocubes and the nanospheres in this study.

Table 1 shows that the calculated average EFs were consistently larger for the nanocubes compared with the nanospheres. This result was in agreement with our previous work comparing nanocubes and truncated nanocubes (cubes with the corners attenuated by etching), where the nanoparticles with sharper features gave larger average EFs.[33] Table 1 also shows that 1,4-BDT and 4-MBT had a significantly larger average EF as compared with 1-PT for both nanoparticles. The average EFs calculated for 1,4-BDT and 4-MBT were similar for the nanocubes but different for the nanospheres, with the 1,4-BDT having a larger average EF. There was no clear trend that

TABLE 1: Average Enhancement Factors Calculated for the Nanocubes of 38 nm in Edge Length and Nanospheres of 35 nm in Diameter Used in This Study[a]

molecule	orientation	band[b]	mode	nanocube	std. dev.	nanosphere	std. dev.
1,4-BDT	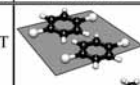	1561	8a A_g	5.8×10^5	2.7×10^2	5.7×10^2	1.7×10^2
		1183	9a A_g	6.6×10^5	1.1×10^3	8.1×10^2	9.8×10^1
4-MBT	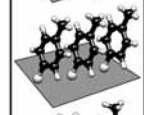	1593	8a A_g	5.5×10^5	9.4×10^2	2.6×10^2	9.4×10^1
		1072	7a A_g	5.9×10^5	2.7×10^2	3.8×10^2	6.8×10^1
1-PT	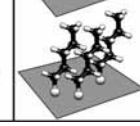	706	$(C\text{-}S)_t$	9.2×10^4	8.3×10^1	1.5×10^2	1.1×10^1
		890	$(CH_3)_{rock}$	3.9×10^4	1.9×10^2	9.9×10^1	1.8×10^1

[a] The average EFs were calculated for the 8a vibrational mode (1561 cm^{-1}) and the 9a vibrational mode (1183 cm^{-1}) of 1,4-benzenedithiol (1,4-BDT), the 8a vibrational mode (1593 cm^{-1}) and the 7a vibrational mode (1072 cm^{-1}) of 4-methylbenzenethiol (4-MBT), and the S−C stretching mode (706 cm^{-1}) and the CH_3 rocking mode (890 cm^{-1}) of 1-pentanethiol (1-PT). All experiments used a 514 nm excitation laser and were performed in water. [b] Wavenumber in cm^{-1}. The molecular footprint, or area occupied by the molecules on the metal surface, were 0.54 nm^2 for 1,4-BDT, 0.19 nm^2 for 4-MBT, and 0.21 nm^2 for 1-PT and were taken from refs 24, 50, and 51 respectively.

connected the molecular geometry to the magnitude of the EF based solely on the symmetries of the Raman tensors of the various bands studied. This was expected, as it is difficult to connect molecular geometries solely to the SERS EF primarily because this dependence has proven to be inconsistent and hard to establish experimentally.[30,34] Nor did the calculated average EFs show a clear relationship between the Stokes wavelengths (the bands identified in Table 1) and the wavelength of excitation laser. It is well-known that SERS EFs have two multiplicative contributions from the underlying plasmon resonance, one at the laser wavelength and the other at the Stokes wavelength (the scattered photons).[35] The EF decreases as the difference between these frequencies increases. The fact that the average EFs calculated herein do not show this trend supports a fixed adsorption geometry for the molecules studied,[8] or, simply, that this effect was too weak to be detected.

The larger average EFs calculated for the nanocubes relative to the nanospheres can be readily understood in terms of particle shape and near-field properties. While size also plays a role in the EF of a nanoparticle, for the particles compared in Table 1, nanocubes of 38 nm in edge length and nanospheres of 35 nm in diameter, the size difference was not significant enough to contribute to the large discrepancy in average EFs of these two particles. A nanoparticle's size is expected to affect its ability to enhance Raman signals.[35] This dependency is valid for nanoparticles under 100 nm, where larger nanoparticles will enhance Raman signals more than smaller nanoparticles with all else being equal. Our results suggest that size dependency does not contribute to the large difference between the EFs for the nanocubes and nanospheres discussed in this study. In Figure 4, the SERS spectra from larger nanocubes (46 nm in edge length) are shown, and the average EFs for 1,4-BDT and 4-MBT are shown in Table 2. We found the average EFs calculated from the nanocubes of 46 nm in edge length to be consistent with those from the nanocubes 38 nm in edge length as well as the SERS band morphologies. These results indicate that shape plays a much more important role in maximizing the EF compared with a size difference of ~10 nm for nanocubes.

It is well-established that the shape of a nanoparticle affects its near-field properties, and these near-field properties, in turn,

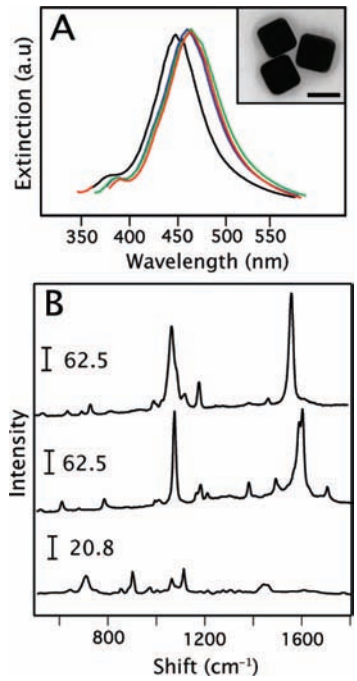

Figure 4. Extinction spectra and SERS spectra from Ag nanocubes with an average edge length of 46 ± 6 nm: (A) The far-field extinction spectra for the Ag nanocubes (black line) and after functionalization with 1,4-BDT (red line), 4-MBT (green line), and 1-PT (blue line). All spectra were taken in water after sonication. The inset shows the TEM image of the Ag nanocubes where the scale bar is 50 nm. For these nanocubes, the main extinction peak was located at 450 nm and was red-shifted ~15 nm after functionalization with the thiolate SAMs. (B) SERS spectra taken from nanocubes in part A for three different molecules: 1,4-BDT (top trace), 4-MBT (middle trace), and 1-PT (bottom trace). The numbers above each spectrum represents the scale in adu mW^{-1} s^{-1}.

TABLE 2: Average Enhancement Factors for 1,4-BDT and 4-MBT Adsorbed on Nanocubes of 46 nm in Edge Length[a]

molecule	band[b]	mode	nanocube	std dev
1,4-BDT	1561	8a A_g	5.7×10^5	5.8×10^3
	1183	9a A_g	4.9×10^5	4.4×10^3
4-MBT	1593	8a A_g	6.1×10^5	8.4×10^3
	1072	7a A_g	4.4×10^5	7.7×10^3

[a] The average EFs were calculated for the 8a vibrational mode (1561 cm^{-1}) and the 9a vibrational mode (1183 cm^{-1}) of 1,4-BDT and the 8a vibrational mode (1593 cm^{-1}) and the 7a vibrational mode (1072 cm^{-1}) of 4-MBT. [b] Wavenumber in cm^{-1}.

are believed to affect the SERS activity of a particular system.[35] This can be seen through the simulation in Figure 5, where the electric field enhancement (|*E*|) contours are plotted around Ag nanocubes and Ag nanopheres. The near-field properties of the nanocubes and the nanospheres were computed to allow for a direct comparison between the theoretical and experimental results. The DDA method was used to calculate the distribution and intensity of the electric field enhancement surrounding a Ag nanocube (38 nm in edge length), and Mie theory was used to calculate the electric field enhancement of a Ag nanosphere (35 nm in diameter). Figure 5A shows the |*E*| contours with the laser polarized along the [110] direction of the nanocube. As we have previously shown, laser polarization can have significant affects on the SERS of a nanocube;[36] however, in this study the cubes are suspended in solution with no fixed orientation. Therefore, combining the field distributions over many orientations and averaging them over the particle surface will result in an average value that can be used to predict the experimentally determined average EF for each particle (as the SERS EF is proportional to the fourth-power of the electric field enhancement for simple systems).[37,38] The average EF was calculated to be 4.8×10^4 at 0.5 nm above the cube surface. In contrast, as readily seen in Figure 5B, the sphere had much lower |*E*| contours with an average EF of 1.2×10^2 at 0.5 nm above the surface. These estimates do not take into account the molecules used in this study and hence only predict the electromagnetic enhancement contribution to the measured EF. Research has shown that SERS is a combination of two effects, namely the electromagnetic enhancement and the chemical enhancement.[35,39] The chemical enhancement is dependent on the interaction between the molecule and the metal surface and is generally thought to contribute to the overall EF by a few orders of magnitude (10−100). The electromagnetic enhancement is thought to be the major contributor to SERS (with enhancements as large as $\sim 10^{10}$) and, as noted above, is dependent on the near-field properties generated by plasmon effects, which are sensitive to many parameters including the shape of the metal nanoparticle.

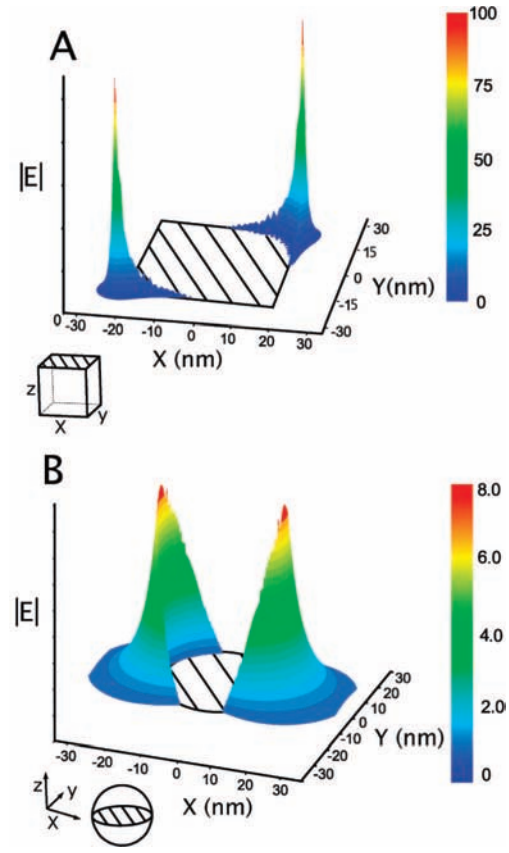

Figure 5. Electric field enhancement (|*E*|) contours for a Ag nanocube of 38 nm in edge length and a Ag nanosphere of 35 nm in diameter with an excitation wavelength of 514 nm and with water as the external dielectric medium. The cartoon at the bottom of each contour plot shows the plane of the nanoparticle represented by the calculated |*E*| contour plot. For part A, the incident light is along the *z*-axis and the *E*-field along the [110] direction, and for part B, the incident light is along the *z*-axis and the *E*-field along the *x*-axis. For the cube, the *E*-field enhancement is localized at the corners.

The dependency of the near-field properties on shape can be understood in terms of the LSPR. The LSPR is the collective oscillation of the conduction electrons of a metallic nanoparticle induced by light.[40] It is known that the LSPR peaks of nanoparticles with sharp features will be red-shifted with respect to smooth nanoparticles, as seen in Figure 2. This red-shift

reflects an attenuation of the rate of plasmon oscillation and is understood to be caused by the accumulation of the surface electrons to the sharp features of the nanoparticle, effectively increasing charge separation and reducing the restoring force for electron oscillation.[41] This is readily seen in the DDA calculations in Figure 5A, where the *E*-field, produced by the oscillation of surface electrons, is confined to the corners of the nanocube, greatly increasing the *E*-field intensity and the SERS activity of the nanocubes compared with the nanospheres.

Besides the larger measured average EF for the nanocubes, another general observation of Table 1 was the larger than predicted average EF for nearly all molecule-substrate combinations (except for 1-PT on Ag nanospheres). We have considered the possibility that hot spots might have formed in solution due to nanoparticle aggregation and this was the origin of the larger than predicted average EF for both the nanocubes and nanospheres. While there was surely some aggregation in each sample, there are several factors that eliminate this possibility. The first is the highly uniaxial nature of the coupling of hot spots with the incident laser polarization and the fact that dimers, trimers, or other clusters are moving randomly in solution, so this coupling is exceedingly rare and transitory.[42] Also, the disparity between the predicted and measured average EF varies from ~14 to ~1.2 with the aromatic groups giving much larger average EFs and the average EF for 1-PT being typically ~2 times greater than expected. Contributions to the SERS from aggregation would be more consistent, as hot spots typically report EFs with a magnitude near 10^8. Finally, aggregation was not readily seen in the solution or the SEM (besides what can be expected from capillary interactions during sample drying), and the LSPR spectra support that there was no significant aggregation in the suspension (see Supporting Information).

These results suggest that there was possibly some chemical contribution to the measured average EFs and this is why the measured values are greater than predicted by theory, which accounts only for electromagnetic enhancement. This was further supported by the band shapes and intensities of the molecules used in this study, which were significantly different for the nanocubes and nanospheres, as seen in Figure 3. The chemical enhancement in SERS comes from the modification of the Raman polarizability of the molecule by direct electronic interaction with the metal surface. The chemical contribution can be understood from two different aspects. The first is the CHEM enhancement, which is primarily ground-state chemical interactions between the molecule and nanoparticle that do not include excitations and are dependent on polarizability (a static chemical enhancement), and the second is the CT enhancement, where the excitation wavelength is resonant with nanoparticle−molecule charge-transfer transitions.[39] For this experiment, it was impossible to separate these two contributions, but because the CHEM enhancement is predicted to be fairly modest (~10), it is probably coupled with the CT enhancement. As noted above, the disparity between the average EFs of the nanocubes and nanospheres is larger than predicted, by a factor of ~6 for 4-MBT and ~3 for 1,4-BDT. The difference in the measured average EFs of the nanocubes and nanospheres compared with theory is interesting. We believe that sharp corners on metallic nanoparticles are not only locations of strong *E*-field intensities but are also special sites that can give rise to larger CHEM enhancements relative to smooth surfaces or highly coordinated areas. As recently demonstrated with Ag and Au clusters,[43,44] pyridine that was adsorbed to the corner of the cluster was predicted to have a larger CHEM enhancement when compared with the surface. For the silver cluster, these chemical enhancements were on the order of 8 and 4 for pyridine adsorbed at the corner and the surface, respectively. This was consistent with our observations for 1-PT, where the discrepancy between the predicted and calculated average EF for the 1-PT C−S stretching mode was ~2 for the nanocubes. For the nanospheres the difference was not significant considering the error involved in the measurement, nor were the CH_3 rocking modes found to be significantly different than predicted for either particle. For 1,4-BDT and 4-MBT, it is possible that the CHEM enhancement contributed to some of the additional enhancement, but for these molecule−particle combinations the measured EF was greater than predicted by a much larger factor.

For 1,4-BDT and 4-MBT, our results suggest that sharp features can lead to a greater CT enhancement. For 1,4-BDT thiolate, the broadening of the 1058 and 1085 cm^{-1} bands into one large band near ~1066 cm^{-1}, when adsorbed on to the nanoparticles, is indicative of surface−molecule π interactions.[24,45] This is readily seen in Figure 3A for the nanocubes and nanospheres. For 4-MBT, the benzene ring breathing modes were also broadened relative to the normal Raman spectrum; however, these bands did not undergo broadening to the extent of 1,4-BDT. This distinction is important, because for the CT enhancement, the degree to which the benzene π orbitals are spatially related to the metal surface is thought to be directly related to the amount of vibronic coupling between these orbitals and the metal surface: the more coupling, the larger the SERS EF.[46] For benzene and its derivatives, broadening (and to a lesser extent red-shifting) of the ring breathing modes can be considered evidence for surface−π orbital interaction.[30,45] Furthermore, some of these bands are often seen as "blinking" in single molecule SERS and are believed to be indicators of charge transfer or wave function mixing between the π orbitals and the metal surface.[39] This blinking phenomenon can be understood in terms of the change in spatial orientation of the molecule, where CT enhancement occurs with a magnitude proportional to how well the molecular π orbitals can couple with metal surface.[47] While no blinking was observed in this experiment (nor was any expected), some modes were found to be sensitive to the nanoparticle morphology and were selectively enhanced (that is, the particular mode was more enhanced than the majority of other modes) or appeared only with certain nanoparticle morphology. For the aromatic thiolates in this study, the spectra in Figure 6 suggest that there is more π orbital coupling to the Ag surface of the nanocubes as opposed to the nanospheres. For 1,4-BDT, this is readily seen in Figure 6A, where the fundamental benzene ring breathing mode 1 is split into a doublet for the normal Raman (peaks 1085 and 1058 cm^{-1}) and are merged into one feature for the sphere, indicating that both peaks have substantially broadened. For the cubes, these peaks have continued to broaden to form a single band at 1066 cm^{-1}, indicating more surface−π orbital interaction as compared with the nanosphere. In general, all the SERS bands associated with ring breathing modes were broader compared with the normal Raman of the 1,4-BDT anion; however, the extent of the broadening varied considerably.

Similar to 1,4-BDT, this broadening trend was consistent for 4-MBT as seen in Figure 6B for the ring breathing mode 8a (1593 cm^{-1}). Although, contrasting the peak area of the 1593 cm^{-1} band for the nanosphere and nanocube, it is not clear if there is substantial broadening of the band at 1593 cm^{-1} or if the broadening is primarily due to the selective enhancement of the 8b mode at 1578 cm^{-1}. While the 1578 cm^{-1} peak could not be used to calculate the average EF (this peak is not present in the normal Raman spectrum), contrasting this peak area

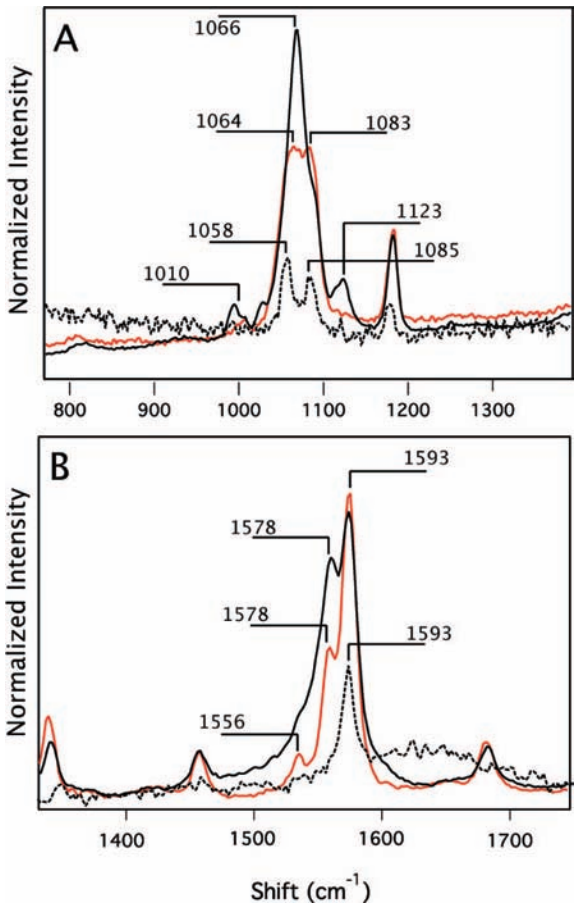

Figure 6. SERS spectra of (A) 1,4-BDT and (B) 4-MBT adsorbed on Ag nanocubes (black) and Ag nanospheres (red) and the normal Raman spectra (dotted). These spectra have been normalized to compare band shapes and are averages of five spectra to show the consistency of peak morphology. Peak frequencies in cm^{-1} are shown for clarity.

between the Ag nanocubes and Ag nanospheres gives a factor of ~1.5, indicating the sensitivity of this band to particle morphology. Furthermore, this b_2 in-plane mode has been associated with the CT enhancement for the molecule 4-aminobenzenethiol (4-ABT) as well as other b_2 bands.[48] For the SERS of 4-MBT on nanocubes, the 1578 cm^{-1} b_2 mode showed a selective enhancement and broadening, merging with the band at 1556 cm^{-1}, as seen in Figure 6B. Other bands associated with b_2 modes observed for 4-MBT in this study, 1157 and 1371 cm^{-1}, did not follow a clear trend in terms of selective enhancement. For the 1,4-BDT, the bands at 1010 and 1123 cm^{-1} were selectively enhanced for the Ag nanocubes. These bands, which we assigned to 18a and 18b modes, are also in-plane vibrations.[30] For both 1,4-BDT and 4-MBT, the selective enhancement and broadening of these bands is evidence for CT enhancement and suggests a greater coupling between the metal surface and the molecule for nanocubes as opposed to nanospheres. This was consistent with the average EF calculations. The average EFs reported for the nanocubes were on average ~10 times greater than predicted, while the average EFs for the nanospheres were on average ~2 times greater than predicted. This dependency is seen plainly with the molecule 4-MBT. As shown in Figure 5A, nearly all of the enhancement for the nanocube will occur near the corners of the particle. Since corners are also where significant defects in monolayers are located,[49] we expect these defect sites to allow for the parallel or flat adsorption of 4-MBT, leading to a larger CT enhancement. This is why the 4-MBT has an average EF similar to that of 1,4-BDT when chemisorbed onto the nanocubes but not the nanospheres. The nanospheres do not have the sharp features that not only disrupt the monolayer and promote more coupling between the molecule and the metal surface but also localize the *E*-fields at these locations.

Conclusion

For Ag nanoparticles with a similar size and far-field properties, we found that particles with sharp nanoscale features on the surface provided a greater SERS enhancement. This dependency was made clear through near-field calculations, where large *E*-field enhancements were found at the sharp corners of the nanocubes used in this study. We also found evidence to suggest that these features imparted a greater chemical enhancement contribution to the overall SERS signal based on quantitative calculations and the band morphology of benzene ring modes. The larger chemical enhancement from sharp features can be understood in terms of the interaction between the molecule and the metal surface. The thiolate SAMs used in this study form readily on both the nanocubes and nanospheres, however, nanoparticle features that are sharp have intrinsically fewer cohesive neighbors and are, therefore, relatively higher energy. These regions coordinate more strongly with adsorbed molecules and cause defects in the monolayers, increasing the propensity for nanoparticle−molecule interactions that can lead to greater chemical enhancements for SERS. Shape therefore plays an important role in SERS, not only in terms of localizing *E*-fields at sharp features, but also in terms of surface chemistry and the molecule−surface interaction. Our data confirms that sharp features should be included in the design of hot spots in order to take advantage of this useful property.

Acknowledgment. This work was supported in part by the NSF through a research grant from DMR (0804088) and the NIH through a 2006 Director's Pioneer Award (5DP1OD000798-03). We thank the Jens Environmental Molecular and Nanoscale Analysis Laboratory at Washington University in St. Louis for the ICP-MS analysis and the Center for Materials Innovation at Washington University in St. Louis for use of the HRTEM microscope.

Supporting Information Available: Tables S1−S3. This material is available free of charge via the Internet at http://pubs.acs.org.

References and Notes

(1) Jeanmaire, D. L.; Van Duyne, R. P. *J. Electroanal. Chem.* **1977**, *84*, 1.
(2) Kneipp, K.; Kneipp, H.; Itzkan, I.; Dasari, R.; Feld, M. *Chem. Rev.* **1999**, *99*, 2957.
(3) Kneipp, J.; Kneipp, H.; Kneipp, K. *Chem. Soc. Rev.* **2008**, *37*, 1052.
(4) Stuart, D.; Yuen, J.; Shah, N.; Lyandres, O.; Yonzon, C.; Glucksberg, M.; Walsh, J.; VanDuyne, R. *Anal. Chem.* **2006**, *78*, 7211.
(5) Qin, L.; Banholzer, M.; Millstone, J.; Mirkin, C. A. *Nano Lett.* **2007**, *7*, 3849.
(6) Banholzer, M. J.; Millstone, J. E.; Qin, L.; Mirkin, C. A. *Chem. Soc. Rev.* **2008**, *37*, 885.
(7) Natan, M. J. *Faraday Discuss.* **2006**, *132*, 321.
(8) LeRu, E.; Blackie, E.; Meyer, M.; Etchegoin, P. *J. Phys. Chem. C* **2007**, *111*, 13794.
(9) Kneipp, K.; Wang, Y.; Kneipp, H.; Perelman, L. T.; Itzkan, I.; Dasari, R. R.; Feld, M. S. *Phys. Rev. Lett.* **1997**, *78*, 1667.
(10) Nie, S.; Emory, S. R. *Science* **1997**, *275*, 1102.
(11) Kelly, K.; Coronado, E.; Zhao, L.; Schatz, G. C. *J. Phys. Chem. B* **2003**, *107*, 668.
(12) Hao, E.; Schatz, G. C. *J. Chem. Phys.* **2004**, *120*, 357.
(13) Zou, S.; Schatz, G. C. *Chem. Phys. Lett.* **2005**, *403*, 62.
(14) Wang, Z.; Pan, S.; Krauss, T. D.; Du, H.; Rothberg, L. J. *Proc. Natl. Acad. Sci. U.S.A.* **2003**, *100*, 8638.

(15) Qin, L.; Zou, S.; Xue, C.; Atkinson, A.; Schatz, G. C.; Mirkin, C. A. *Proc. Natl. Acad. Sci. U.S.A.* **2006**, *103*, 13300.
(16) Orendorff, C. J.; Gearheart, L.; Jana, N. R.; Murphy, C. J. *Phys. Chem. Chem. Phys.* **2006**, *8*, 165.
(17) Yang, Y.; Matsubara, S.; Xiong, L.; Hayakawa, T.; Nogami, M. *J. Phys. Chem. C* **2007**, *111*, 9095.
(18) Jackson, J. B.; Halas, N. J. *Proc. Natl. Acad. Sci. U.S.A.* **2004**, *101*, 17930.
(19) Skrabalak, S. E.; Au, L.; Li, X.; Xia, Y. *Nat. Protoc.* **2007**, *2*, 2182.
(20) Kim, M. H.; Lu, X.; Wiley, B.; Lee, E. P.; Xia, Y. *J. Phys. Chem. C* **2008**, *112*, 7872.
(21) Afseth, N. K.; Segtnan, V. H.; Wold, J. P. *Appl. Spectrosc.* **2006**, *60*, 1358.
(22) Taylor, C. E.; Pemberton, J. E.; Goodman, G. G.; Schoenfisch, M. H. *Appl. Spectrosc.* **1999**, *53*, 1212.
(23) Sauer, G.; Brehm, G.; Schneider, S. *J. Raman Spectrosc.* **2004**, *35*, 568.
(24) Joo, S. W.; Han, S. W.; Kim, K. *J. Colloid Interface Sci.* **2001**, *240*, 391.
(25) Bryant, M. A.; Pemberton, J. E. *J. Am. Chem. Soc.* **1991**, *113*, 3629.
(26) Yang, W.-H.; Schatz, G. C.; Duyne, R. P. V. *J. Chem. Phys.* **1995**, *103*, 869.
(27) Xia, Y.; Xiong, Y.; Lim, B.; Skrabalak, S. E. *Angew. Chem. Int. Ed.* **2009**(in press).
(28) Wiley, B.; Sun, Y.; Xia, Y. *Acc. Chem. Res.* **2007**, *40*, 1067.
(29) Zhou, F.; Li, Z.-Y.; Liu, Y.; Xia, Y. *J. Phys. Chem. C* **2008**, *112*, 20233.
(30) Cho, S. H.; Han, H. S.; Jang, D.-J.; Kim, K.; Kim, M. S. *J. Phys. Chem.* **1995**, *99*, 10594.
(31) Carron, K. T.; Hurley, L. G. *J. Phys. Chem.* **1991**, *95*, 9979.
(32) Love, J.; Estroff, L.; Kriebel, J.; Nuzzo, R.; Whitesides, G. *Chem. Rev.* **2005**, *105*, 1103.
(33) McLellan, J. M.; Siekkinen, A.; Chen, J.; Xia, Y. *Chem. Phys. Lett.* **2006**, *147*, 122.
(34) Osawa, M.; Matsuda, N.; Yoshii, K.; Uchida, I. *J. Phys. Chem.* **1994**, *98*, 12702.
(35) Moskovits, M. *J. Raman Spectrosc.* **2005**, *36*, 485.
(36) McLellan, J.; Li, Z.-Y.; Siekkinen, A.; Xia, Y. *Nano Lett.* **2007**, *7*, 1013.
(37) Gersten, J.; Nitzan, A. *J. Chem. Phys.* **1980**, *73*, 3023.
(38) Le Ru, E. C.; Etchegoin, P. G. *Chem. Phys. Lett.* **2006**, *423*, 63.
(39) Jensen, L.; Aikens, C. M.; Schatz, G. C. *Chem. Soc. Rev.* **2008**, *37*, 1061.
(40) Xia, Y.; Halas, N. J. *MRS Bull.* **2005**, *30*, 338.
(41) Wiley, B. J.; Im, S. H.; Li, Z.-Y.; McLellan, J.; Siekkinen, A.; Xia, Y. *J. Phys. Chem. B* **2006**, *110*, 15666.
(42) Ru, E. C. L.; Meyer, M.; Blackie, E.; Etchegoin, P. G. *J. Raman Spectrosc.* **2008**, *39*, 1127.
(43) Zhao, L.; Jensen, L.; Schatz, G. C. *J. Am. Chem. Soc.* **2006**, *128*, 2911.
(44) Aikens, C.; Schatz, G. C. *J. Phys. Chem. A* **2006**, *110*, 13317.
(45) Gao, P.; Weaver, M. J. *J. Phys. Chem.* **1985**, *89*, 5040.
(46) Campion, A.; Kambhampati, P. *Chem. Soc. Rev.* **1998**, *27*, 241.
(47) Wang, Z.; Rothberg, L. *J. Phys. Chem. B* **2005**, *109*, 3387.
(48) Fromm, D. P.; Sundaramurthy, A.; Kinkhabwala, A.; Schuck, P. J.; Kino, G. S.; Moerner, W. E. *J. Chem. Phys.* **2006**, *124*, 061101.
(49) Sun, L.; Crooks, R. M. *Langmuir* **1993**, *9*, 1951.
(50) Tao, Y.-T.; Wu, C.-C.; Eu, J.-Y.; Lin, W.-L.; Wu, K.-C.; Chen, C.-H. *Langmuir* **1997**, *13*, 4018.
(51) Laibinis, P. E.; Whitesides, G. M.; Allara, D. L.; Tao, Y.-T.; Parikh, A. N.; Nuzzo, R. G. *J. Am. Chem. Soc.* **1991**, *113*, 7152.

JP8101817